Development of a Vortex Flow Pancake Hybrid Rocket Engine

Mohanad F. Warrayat[*], Nathan C. Renard[†], Evan C. Holt[‡], Alex W. L. Pimlott[§], Garrett Rand[¶], Samuel D. Bolar[‖], and Ryan J. Milcarek[**]

Arizona State University, Tempe, AZ, 85287

Historically, the development and implementation of hybrid rocket engines has been hindered by poor regression rate and combustion efficiency. Advancement of such engines would be advantageous in the field of propulsion due to their inherent safety, a function of spatial and phasal separation of the fuel and oxidizer. In this regard, Sun Devil Rocketry's (formerly Daedalus Astronautics) Hybrids Research Team at ASU has developed a Vortex Flow Pancake Hybrid Rocket Engine as a novel alleviation modality. This design incorporates an induced vortex oxidizer flow field between two flat fuel disks. The nature of this flow field increases regression rate and combustion efficiency through its increased turbulent stress and residence time, respectively. The development of this novel engine includes a design of a nitrogen purge system, modification of a data acquisition system, design of piping and instrumentation, and development of an engine. This engine is expected to produce a thrust of approximately 200 lbf, with a chamber pressure of 500 psi.

I. Nomenclature

α	=	nozzle contour angle
$\dot{m}_{ox}$	=	oxidizer mass flow rate
$\dot{m}_{prop}$	=	propellant mass flow rate
γ	=	specific heat ratio
ρ	=	density of nitrous oxide
$A(x)$	=	nozzle area with respect to location
$a(x)$	=	speed of sound with respect to location
A^*	=	cross-sectional area of nozzle throat
A_2	=	total cross-sectional area of injection holes
A_e	=	cross-sectional area of nozzle exit
$C_{p_{Al}}$	=	specific heat of aluminum
$C_{p_{N_2O}}$	=	specific of nitrous oxide
dq	=	heat transferred to aluminum with film cooling
F_{thrust}	=	thrust
g	=	gravity
h_1	=	height at upstream location
h_2	=	height at downstream location
$M(x)$	=	Mach number with respect to location
N_2O	=	nitrous oxide
$P(x)$	=	pressure with respect to location
P_1	=	upstream pressure
P_2	=	downstream pressure
P_∞	=	ambient pressure
P_e	=	nozzle exit pressure

[*]Undergraduate Student, B.S.E. '20, School of Matter, Transport & Energy, AIAA Student Member.

[†]Undergraduate Student, B.S.E. '20, School of Matter, Transport & Energy, AIAA Student Member.

[‡]Undergraduate Student, B.S.E. '22, School of Matter, Transport & Energy, AIAA Student Member.

[§]Undergraduate Student, B.S.E. '20, School of Matter, Transport & Energy, AIAA Student Member.

[¶]Undergraduate Student, B.S.E. '21, School of Matter, Transport & Energy, AIAA Student Member.

[‖]Undergraduate Student, B.S.E. '20, School of Matter, Transport & Energy, AIAA Student Member.

[**]Asst. Professor, School of Matter, Transport & Energy, AIAA Member.

P_t	=	total pressure
q_{Al}	=	heat transfer to aluminum in the absence of film cooling
q_{melt}	=	heat transfer required to melt aluminum
q_{N_2O}	=	heat transfer to nitrous oxide
R	=	gas constant
$T(x)$	=	temperature with respect to location
T_∞	=	ambient temperature
T_{flame}	=	adiabatic flame temperature
T_{melt}	=	temperature at which aluminum melts
T_{N_2O}	=	temperature of nitrous oxide
T_t	=	total temperature
$V(x)$	=	velocity with respect to location
v_1	=	upstream fluid velocity
v_2	=	downstream fluid velocity
V_e	=	nozzle exit velocity

II. Introduction

Mainstream rocket propellants are categorized into three groups: solids, liquids, and hybrids. These groups describe the state of matter of the fuel and oxidizer prior to and during ignition. The contents of this paper are concerned with the research and development of technology in the hybrids propulsion category. Hybrid rocket technology, while still in its infancy, is being investigated as a more viable form of rocket propulsion in order to mitigate complications found in other propulsion systems. Hybrid engines are stable during manufacturing and storage, exhibit a far simpler piping system than liquid systems, and are able to throttle and extinguish mid-ignition, unlike solid propellant systems. Despite its relative absence in industrial applications compared to liquid and solid systems, hybrid propulsion is a promising advancement for the future of rocket propulsion.

Safety is a major design consideration in rocket propulsion research. The hybrid rocket engine has intermittently risen to the forefront of this research due to its safety characteristics. Namely, the separation of fuel and oxidizer alleviates risk of explosions in storage and flight operations. Spatial separation between the fuel and the flame front ensures that any exothermic chemical reactions occur a distance from its surface [1]. Hybrid rocket engines operate with a diffusion flame, whereas the fuel and oxidizer are premixed in solid rocket motors. The nature of this diffusion flame alleviates sensitivity of imperfections of the fuel grain that are seen in solid rocket systems, again because the solid fuel in hybrid rockets does not directly encounter the flame front. This means that hybrid rocket engines do not need to be designed for a maximum expected operating pressure because they would not experience the same magnitude of detrimental pressure fluctuations seen in solid rocket motors with grain imperfections. One disadvantage of the hybrid rocket engine undergoing diffusion flame combustion lies in its inferior solid fuel regression rate. The rate at which the solid fuel is able to regress, mix with the oxidizer, and combust is limited by the rate of diffusion. Hybrid rocket engines exhibit poor combustion efficiency in addition to regression rates that are an order of magnitude smaller than that of solid rocket motors [1]. Due to this deficiency in regression rate, larger hybrid engines typically incorporate a fuel grain with a multiport geometry to contain the necessary burning area.

A potential solution to the common nuisances of hybrid technologies is the Vortex Flow Pancake Hybrid Rocket Engine (VFPHRE). This experimental design introduces a means of mitigating the poor regression rate and decreased combustion efficiency resulting from turbulent stresses and particle residence times of hybrid engines [2]. The vortex flow pattern in the combustion chamber induces shear stress in the fuel-oxidizer interface [3]. The circulating motion of fuel particles around the chamber further increases the regression rate and combustion efficiency of the vortex engine. This particular design is an important step forward in advancing hybrid propulsion systems and rocketry as a whole.

This paper covers the progress made by Sun Devil Rocketry (SDR) in the design and procurement of this novel engine. Particular emphasis is placed on calculations of performance parameters and engine architecture – including piping and instrumentation.

III. VFPHRE Design

A. Engine Configuration

As shown in Fig. 1, the VFPHRE's core consists of five assembled components – the flapjack base, chamber, injection ring, flapjack top, and a nozzle. The chamber acts as a cylindrical casing that holds two fuel disks and the injection ring. It also contains the required inlets for the liquid nitrous oxide and gaseous nitrogen. The injection ring is seated on a lip within the chamber and acts as a cap. This reduces the cross-sectional area experienced by the flow field and induces a vortex pattern as liquid nitrous oxide enters the chamber. This immediate change in cross-sectional area creates a pressure head while also serving to vaporize the nitrous oxide and separate the plumbing conditions from the chamber environment. In order to meet this criteria, it is required that the port of injection's total cross-sectional area be smaller than that of the chamber inlet.

The aforementioned assembly is encapsulated by the flapjack base and flapjack top, thus acting as the VFPHRE's midsection. This midsection is contained by six bolts that run through the outer perimeter of these two encapsulating components, as seen in Fig. 1. Once fastened, these bolts compress the entire assembly together, activating a face gland o-ring pressure seal that is located between the top face of the injection ring and the bottom face of the flapjack top.

There are three components within this assembly that these six bolts do not directly impact: the bottom fuel disk, the top fuel disk, and the nozzle. The bottom fuel disk is solid throughout and lies freely within the chamber. In contrast, the top fuel disk lies atop an internal retaining ring and is annular in nature to leave an opening for the nozzle entrance. Similarly, the nozzle rests atop a lip located along the inner diameter of the flapjack top and is held securely in place by an internal retaining ring located above. This is a carbon graphite, 30-60 conical nozzle with a throat diameter of 0.5 inches and was chosen amongst current SDR stock due to its large throat diameter. This throat diameter is crucial in prevention of overpressurization during ignition.

The engine is held concentric to the load cell, and it is prevented from vibrating or tipping over during its test by four surrounding rods. These rods are confined to toleranced locations using precision pins to maintain the exact configuration shown in Fig. 1.

B. Piping and Instrumentation

As liquid nitrous oxide and gaseous nitrogen are injected into the combustion chamber, each joint face of this assembly must be sealed to ensure that there is no leakage within the system. A series of standardized o-ring grooves [4] have been implemented for each orifice in VFPHRE's design, including connection points between the centralized core and all external connecting features. Thus, as shown in Fig. 2, o-ring seals are located at the pressure transducer port, the nitrogen purge system port, above and below the nitrous vortex-induction groove, and at each connected face. The temperature ranges experienced at these particular locations are not yet known but will directly impact o-ring material selection.

The following components are required to ensure safe delivery and depressurization of both the liquid nitrous oxide and gaseous nitrogen piping systems: pressure gauge, regulator, ball valve, solenoid valve, check valve, and relief valve. Additionally, the liquid nitrous oxide system will incorporate a venturi to measure the mass flow rate of the liquid nitrous oxide and three reducers to increase the fluid velocity prior to entrance into the chamber. The regulator will be used to
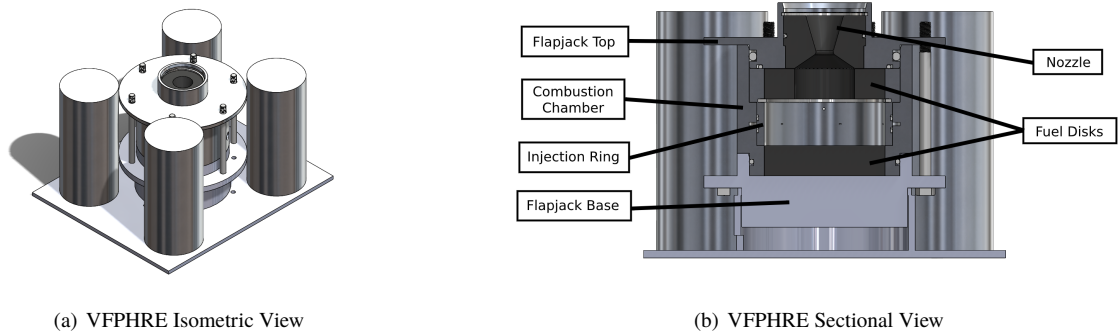

(a) VFPHRE Isometric View

(b) VFPHRE Sectional View

Fig. 1. Isometric View and Labeled Sectional View of the VFPHRE

Fig. 2. VFPHRE O-Ring Placement

(a) Liquid Nitrous Oxide Piping System

(b) Gaseous Nitrogen Piping System
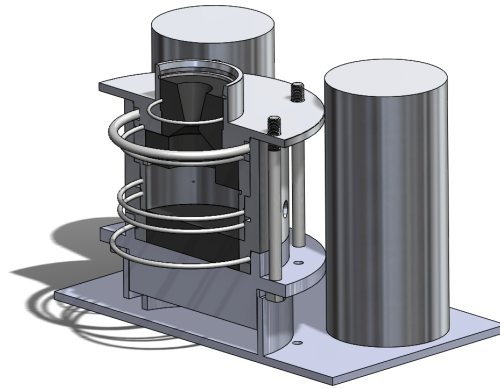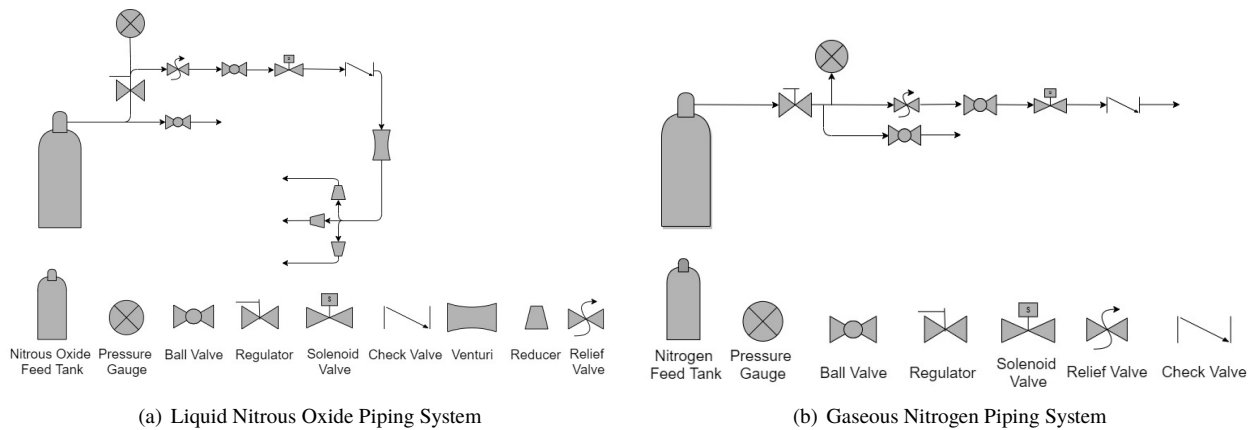
Fig. 3. Piping Systems

maintain delivery of a constant pressure output from the tank. The relief valve serves to relieve any pressure build up of a trapped fluid until it is completely released by the opening of the ball valve to ambient air. Both ball valves are opened prior to the actuation of the solenoid to prime the line. The ball valve exposed to ambient air is then closed, and the fluid will be delivered once the solenoid is activated. The check valve ensures that the flow is one-directional and nothing propagates back to the tank. Schematics of both piping systems are shown by Fig. 3.

IV. Experimental Testing Apparatus

The data acquisition (DAQ) system utilizes a thermocouple (TC), load cell (LC), and three pressure transducers (PTs) which obtain data at the venturi flowmeter, combustion chamber, and the load engine baseplate. SDR's Hybrids Research Team has built upon the organization's current DAQ box, which has evolved over multiple generations of SDR projects, by implementing the previously absent ability to measure temperature. In order to measure the higher resolution TC readings, a new DAQ has been added to the box – namely the NI TC-01. This upgraded DAQ system contains five measurement instrumentation ports, a NI USB-6000 DAQ for PT and LC readings, and a RQ-65D power supply. These upgrades are shown in Fig. 4. A LabView program runs in conjunction with these sensors to receive input signals, most of which are sent from the venturi flowmeter. This attachment to the piping system contains two PT ports, a TC port, and can monitor both the mass flow rate and the state of matter of the oxidizer. As all sensor data is received, it is processed and converted from voltage signals to readings of force, temperature, and pressure. This allows us to monitor the data graphically in real time, which is necessary to ensure safe operation.

In addition to safety precaution, this collected data characterizes engine performance via the following: solid fuel
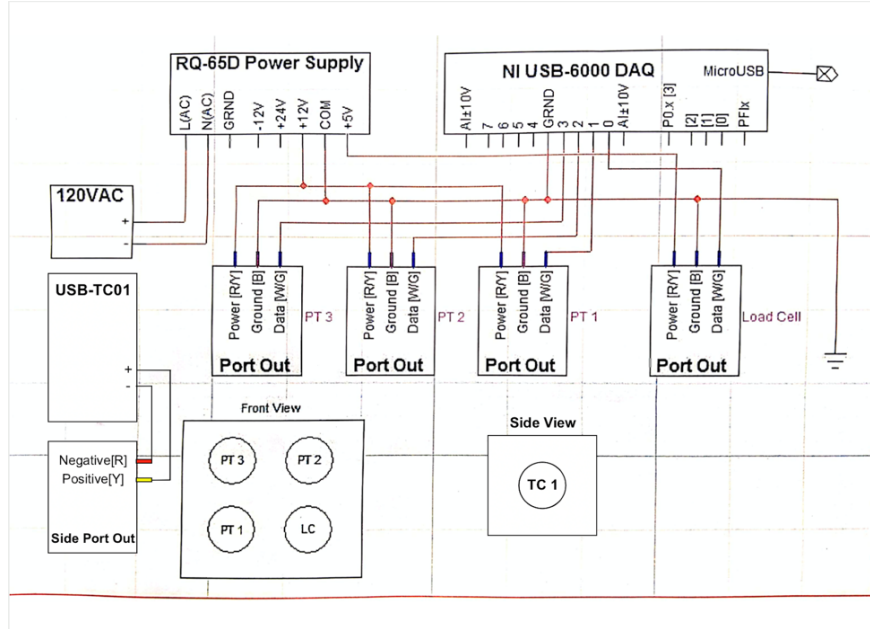
Fig. 4. Data Acquisition Schematic

regression rate, chamber pressure, oxidizer flow rate, thrust, and burn time. Additional validation of this research can be found through comparison between the aforementioned characteristics of the VFPHRE and those of other traditional hybrid engine designs.

V. Calculations of Performance Parameters

A. Mass Flow Rates

The mass flow rate of the oxidizer is the driving parameter in hybrid rocket engines. This mass flow rate influences the solid fuel regression and, thus, the fuel mass flow rate [5]. In this configuration, the oxidizer mass flow rate is dictated by tank pressure. Therefore, the tank pressure is a driving force throughout the entirety of the test. Liquid nitrous oxide can be used as the oxidizer without an inert pressurant. As a result, the tank pressure will decrease as the test progresses. This is beneficial in providing experimental data of thrust as a function of oxidizer mass flow rate.

The expected mass flow rates were calculated assuming incompressible flow of the liquid oxidizer from the tank up to the combustion chamber and that stoichiometric combustion occurred. Mass flow rate of the oxidizer was calculated first, as it is only dependent on tank pressure. Mass flow rate of fuel was then calculated, as it depends on the mass flow rate of the oxidizer. The velocity of the oxidizer is calculated using Bernoulli's equation, Eq. (1). Bernoulli's equation holds here because the nitrous oxide is in a liquid state, therefore the flow is incompressible.

$$P_1 + \rho g h_1 + \frac{1}{2}\rho v_1^2 = P_2 + \rho g h_2 + \frac{1}{2}\rho v_2^2 \tag{1}$$

The height difference is negligible and the velocity of the nitrous oxide in the tank is zero before it starts flowing. Eq. (1) can be rearranged to solve for velocity in Eq. (2), where location 1 is the tank and location 2 is the combustion chamber.

$$v_2 = \sqrt{\frac{2\left(P_1 - P_2\right)}{\rho}} \tag{2}$$

Using the velocity found in Eq. (2), the known density of nitrous oxide, and the cross-sectional area of the piping, the mass flow rate of the oxidizer can be determined by Eq. (3).

$$\dot{m}_{ox} = \rho A_2 v_2 \tag{3}$$

The mass flow rate of the fuel was derived with respect to the oxidizer mass flow rate and the oxidizer to fuel ratio (OFR), assuming stoichiometric combustion. Stoichiometric analysis of the fuel and oxidizer could not be conducted due to the inability to model the fuel casted at SDR. Instead, the stoichiometric OFR is taken to be 7.1 from Ref. [1].

The propellant mass flow rate is a sum of the oxidizer and fuel mass flow rates and can therefore be expressed as a function of the oxidizer mass flow rate and the OFR.

$$\dot{m}_{prop} = \frac{\dot{m}_{ox}\,(1+OFR)}{OFR} \tag{4}$$

This propellant mass flow rate is the maximum achievable mass flow rate through the combustion chamber due to the pressure difference between the nitrous oxide tank and chamber pressure. With an optimally designed nozzle, the choked mass flow rate through the nozzle will match the maximum mass flow rate of the product gas in the combustion chamber. This optimal throat area was assumed for the calculations of thrust. Due to the size constraints of the engine design, the optimal exit area to provide fully expanded flow could not be reached.

B. Thrust

The instantaneous thrust of the VFPHRE will be the force produced at any given time by expelling the propellant from the combustion chamber through a nozzle. To approximate this value, the flow through the nozzle is assumed to be isentropic with no shocks and follow Rayleigh flow in the combustion chamber. Better approximations can be made using a relative efficiency model, but these would require rigorous testing of the VFPHRE or a similar scaled model. The assumption of isentropic conditions throughout the nozzle is reasonable for tests performed at this stage as they provide preliminary base calculations with reasonable accuracy from known parameters, namely tank pressure and the nozzle area profile.

Since the nozzle is conic, its geometry is characterized using two linear fits from three points, those being the entrance, throat, and exit areas. Due to their angled shape, conic nozzles produce diverging flow at the exit. This loss of thrust due to the divergence can be accounted for by adding a modifying term to the thrust equation, Eq. (5), resulting in Eq. (6).

$$F_{thrust} = \dot{m}_{prop}V_e + (P_e - P_\infty)\,A_e \tag{5}$$

$$F_{thrust} = \left(\frac{1+\cos(\alpha)}{2}\right)\dot{m}_{prop}V_e + (P_e - P_\infty)\,A_e \tag{6}$$

To determine the conditions of the product gas in the combustion chamber, the program PROPEP [6] (Propellant Performance Evaluation Program) was used. The masses of the fuel grain and oxidizer were inputted, along with the ambient temperature of the ingredients, chamber pressure, and exhaust pressure. The exhaust pressure was set to be atmospheric and the chamber pressure was set to a range of values. That range was set from max tank pressure to half of max tank pressure. The resulting chamber pressure was then said to be 30 percent of the tank pressure due to pressure losses in the piping and injector. This is relative to previous tests done at SDR, but a more accurate value of chamber pressure will be attained from cold flow testing. From these inputted operating conditions, the specific heat ratio, molecular weight, and total temperature of the propellant gases were found.

The conic nozzle half-angle and exit area are both defined from the nozzle geometry, and the ambient air pressure is dependent upon the specific testing environment (standard atmospheric pressure was assumed for these calculations). Mass flow rate calculations have been shown in the respective section above. Thus, to solve this thrust equation, the flow exit velocity and pressure are both needed. To find these final two unknowns, the Mach number at the nozzle exit must first be determined. This is found using the Mach-area relation, Eq. (7), which relates the Mach number at the exit with the exit-to-throat area ratio.

$$\frac{A(x)}{A^*} = \frac{1}{M(x)}\left[\frac{2}{\gamma+1}\left(1+\frac{\gamma-1}{2}M^2(x)\right)\right]^{\frac{1}{2}\frac{\gamma+1}{\gamma-1}} \tag{7}$$

With this exit Mach number, the temperature of the propellant at the exit can be found using a total-to-static relationship equation for temperature, shown by Eq. (8). The assumption of isentropic flow allows the use of Eq. (9)

to relate the exit temperature to exit pressure, which is needed for Eq. (6). However, this requires the total pressure throughout the nozzle, which can be calculated using the total-to-static relationship for pressure, Eq. (10), at the nozzle inlet. The static pressure at this point can still be considered equal to the static pressure in the combustion chamber. However, the Mach number at this point is also needed to make Eq. (10) a closed equation. In general, as the combustion chamber to throat area ratio increases, the total pressure loss decreases. For area ratios greater than 3, the total pressure loss is approximately zero [7]. For the VFPHRE, the area ratio is approximately 14, therefore the total pressure loss is negligible. The Mach number of the flow in the combustion chamber was determined by Eq. (7) to be 0.06.

$$\frac{T_t}{T(x)} = \left[1 + \frac{\gamma - 1}{2} M^2(x) \right]$$ (8)

$$\frac{P(x)}{P_t} = \left(\frac{T(x)}{T_t} \right)^{\frac{\gamma}{\gamma-1}}$$ (9)

$$\frac{P_t}{P(x)} = \left[1 + \frac{\gamma - 1}{2} M^2(x) \right]^{\frac{\gamma}{\gamma-1}}$$ (10)

With the exit temperature found from Eq. (8), the speed of sound in the propellant medium can be determined using Eq. (11). This result can be directly used in Eq. (12) to find the velocity of the propellant at the nozzle exit.

$$a(x) = \sqrt{\gamma R T(x)}$$ (11)

$$M(x) = \frac{V(x)}{a(x)}$$ (12)

All the variables from Eq. (6) are now known, so a solution can easily be found. Using these variables, the nozzle can be checked to ensure that the flow is choked. The nozzle is choked when the nozzle choking condition is true, which is seen by Eq. (13).

$$\frac{P_t}{P_\infty} \geq \left(\frac{\gamma + 1}{2} \right)^{\frac{\gamma}{\gamma-1}}$$ (13)

This results in a pressure ratio of approximately 1.8. This is true for the VFPHRE because the ratio of combustion chamber total pressure to ambient pressure is between 8 and 16.

The thrust performance of the VFPHRE as a function of the tank pressure can be seen in Fig. 5.

C. Heat Transfer

Heat transfer analysis was conducted, ensuring that the selected materials are capable of withstanding the high combustion temperatures. The chamber walls are shielded from the combustion flames by the entering nitrous oxide. Rudimentary calculations were conducted to verify the efficacy of nitrous oxide's film cooling effect within the system. The specific heat of the nitrous oxide dissipates heat from the combustion flame, preventing the aluminum chamber walls from directly experiencing the full magnitude of flame temperatures.

Heat is transferred to the chamber walls from the flame through the nitrous oxide. The heat transferred through the nitrous oxide is defined by Eq. (14), while the heat transferred through the aluminum, in the absence of the nitrous oxide intermediary, is defined by Eq. (15). The difference between these two equations is defined as the heat transferred to the chamber walls and is shown by Eq. (16).

$$q_{N_2O} = C_{P_{N_2O}} \left(T_{flame} - T_{N_2O} \right)$$ (14)

$$q_{Al} = C_{P_{Al}} \left(T_{flame} - T_\infty \right)$$ (15)
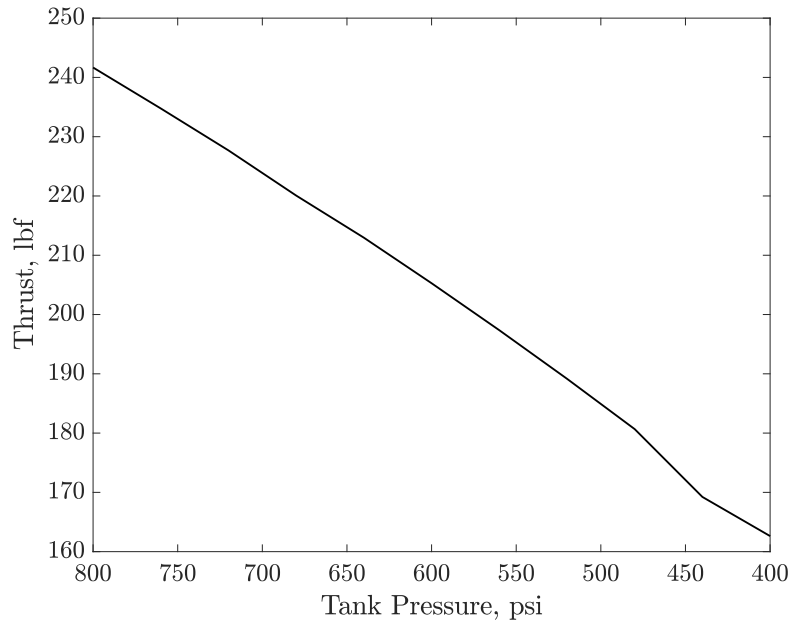
$$dq = q_{Al} - q_{N_2O}$$ (16)

Fig. 5. Thrust as a Function of Nitrous Oxide Tank Pressure

If the chamber walls are exposed to high enough temperatures, the risk of melting arises. Therefore, precaution must be taken to ensure that this does not occur. To mathematically represent and predict the risk of melting, the value obtained for Eq. (14) must not exceed the value obtained in Eq. (17).

$$q_{melt} = C_{p_{Al}} \left(T_{melt} - T_\infty \right) \tag{17}$$

Figure 6 demonstrates how the film cooling effect hinders the melting of the aluminum chamber walls. The heat transfer required to melt the aluminum is avoided for all expected chamber pressures and corresponding adiabatic flame temperatures. Since the burn times are expected to be small, the aluminum walls will not have time to accumulate the heat required to melt.

VI. Conclusions and Future Work

A setup for VFPHRE testing is presented. Calculations needed to size the system and measure performance are discussed. Procession towards the testing phase for the engine is contingent on the completion of the design and manufacturing phases. At present, the majority of the manufacturing of the VFPHRE is finished. However, modifications and refinements are currently taking place in order to ensure the final product is as close to the intended design as possible.

Further VFPHRE design modifications planned by SDR's Hybrids Research Team include multiple new injection rings and varying oxidizer injection angles. First, however, various safety measures and mock-testing phases need to be carried out to guarantee the well-being of team members and the engine itself. Pressure leak testing will commence by pumping pressurized gaseous nitrogen through the plumbing system of the engine. This will confirm the high-pressure tolerance of the piping system. A successful pressure leak test will be followed by a liquid nitrous oxide cold flow test. This test does not include any ignition and provides a safe approach to understanding the functions and operations of each component of the engine – including the expected mass flow rate, pressure head across the injection ring, and the fluid behavior entering the combustion chamber.

The VFPHRE will undergo hot fire testing only after the previous steps are successfully completed, and the necessary safety precautions are understood by all team members. This test puts the engine through the full oxidizer injection and ignition process with the fuel. It is here that data imperative to SDR's research will be obtained, allowing for further iterative design choices to be made to the VFPHRE. The data acquired here will provide insight into the optimization of fuel regression rate and combustion efficiency.
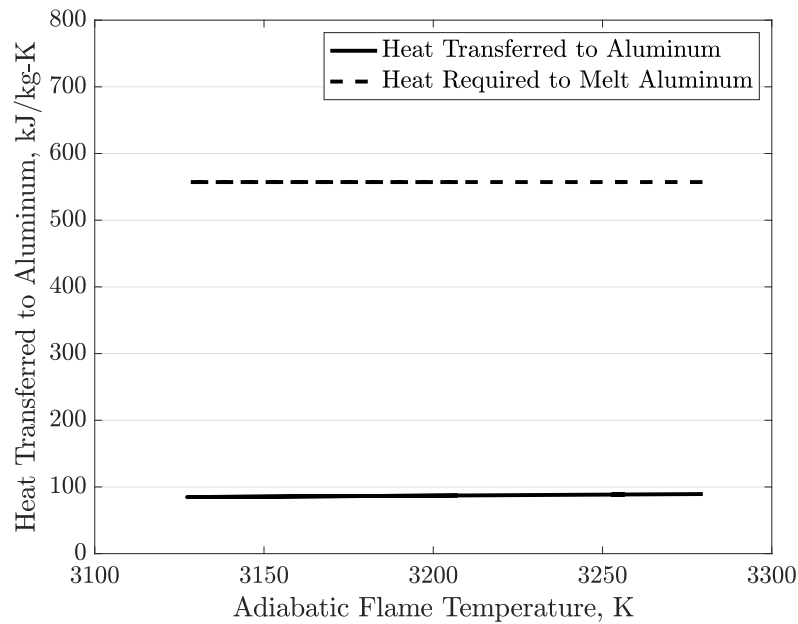
Fig. 6. Adiabatic Flame Temperature vs. Heat Transferred to Aluminum

References

[1] Kuo, K. K., and Chiaverini, M. J., *Fundamentals of hybrid rocket combustion and propulsion*, American Institute of Aeronautics and Astronautics, 2007.

[2] Knuth, W., Gramer, D., Chiaverini, M., and Sauer, J., "Development and testing of a vortex-driven, high-regression rate hybrid rocket engine," *34th AIAA/ASME/SAE/ASEE Joint Propulsion Conference and Exhibit*, 1998, p. 3507.

[3] Jones, C., Myre, D., and Cowart, J., "Performance and analysis of vortex oxidizer injection in a hybrid rocket motor," *45th AIAA/ASME/SAE/ASEE Joint Propulsion Conference & Exhibit*, 2009, p. 4938.

[4] Seals, P., "Parker o-ring handbook (ORD 5700)," *Parker Seal Group, Lexington, KY*, 1992.

[5] Chiaverini, M. J., Serin, N., Johnson, D. K., Lu, Y.-C., Kuo, K. K., and Risha, G. A., "Regression rate behavior of hybrid rocket solid fuels," *Journal of Propulsion and Power*, Vol. 16, No. 1, 2000, pp. 125–132.

[6] Nakka, R., "Richard Nakka's Experimental Rocketry Web Site: Solid Rocket Motor Theory – GUIPEP," 1997. URL http://www.nakka-rocketry.net/th_prope.html.

[7] Hill, P. G., and Peterson, C. R., "Mechanics and thermodynamics of propulsion," *Reading, MA, Addison-Wesley Publishing Co., 1992, 764 p.*, 1992.